

Contact-inhibited chemotactic motility can drive both vasculogenesis and sprouting angiogenesis

Roeland M. H. Merks* and James A. Glazier†
*The Biocomplexity Institute and Department of Physics,
 Indiana University Bloomington, Swain Hall West 159,
 727 E 3rd Street, 47405-7105 Bloomington, IN, USA*

(Dated: November 30, 2018)

Blood vessels can develop either through vasculogenesis, in which endothelial cells—the cells lining the inner walls of arteries and veins—aggregate and form a vascular network, or through angiogenesis: sprouting or splitting of existing blood vessels. Many computational models exist to explain and describe either vasculogenesis or angiogenesis. However, since the same genetic machinery drives both, a plausible mechanism should explain both. Here we present a cell-centered, hybrid Cellular-Potts/Partial Differential Equation Model that reproduces aspects of both sprouting angiogenesis and vasculogenesis. The model assumes that endothelial cells autocrinically secrete a chemoattractant which decays in the extracellular matrix. Vascular network formation requires an additional biologically realistic contact-inhibition mechanism, that represses chemotactic filopodia at cell-cell interfaces (*e.g.* mediated by vascular-endothelial-cadherin). This mechanism also drives a sprouting instability, transforming round cell clusters into vascular networks, a process resembling angiogenesis.

PACS numbers: 87.18.Hf; 87.18.Bb; 87.17.Jj; 89.75.Kd; 61.43.Hv

Blood vessel development is essential for myriad physiological and pathological processes, including wound healing, tumor growth [1, 2] and kidney development [3, 4]. The first step in vascular development is the formation of a network-like pattern, the *primary capillary plexus*. Capillary plexi can form either through *vasculogenesis*, the assembly of disconnected vascular endothelial cells (ECs), or through *angiogenesis*, the sprouting or subdivision of existing blood vessels. Many computational models exist to explain and describe either vasculogenesis [5, 6, 7, 8, 9, 10] or angiogenesis [11, 12, 13]. However, the same genetic machinery regulates angiogenesis and vasculogenesis which are closely related [14], so a plausible mechanism must explain both.

Vascular morphogenesis requires *vascular-endothelial-cadherin* (*VE-cadherin*) [15], which clusters at adherens junctions between endothelial cells and regulates vascular-endothelial growth-factor-A's (*VEGF-A*) effect on ECs; *VEGF-A* is a potent stimulator of angiogenesis. *VE-cadherin* binding dephosphorilates *VEGFR-2* (*VEGFR-2*), which upon *VEGF-A* binding activates the *AKT/protein kinase B (PKB)* pathway, inhibiting cell motility and cell proliferation. *VEGF-A* binding to phosphorylated *VEGFR-2* (*i.e.* in the absence of *VE-cadherin* binding) activates extracellular signal-regulated kinase/mitogen-activated protein kinases (*ERK/MAPK*) [16], including stress-activated protein kinase (*SAPK*)2/p38, inducing actin polymerization and reorganization into stress fibers, triggering cell motility and proliferation in sub-confluent monolayers [16, 17]. Thus, we hypothesize that *VE-cadherin* binding represses chemotactic filopodia at endothelial cell-cell interfaces.

In this letter we show that such contact-inhibition of filopodial extension, in combination with EC autocrine

secretion of a diffusive chemoattractant which decays in the extracellular matrix (*ECM*), may drive a developmental mechanism reminiscent of both vascular web formation and sprouting angiogenesis. We model endothelial cells that a) secrete a chemoattractant; b) preferentially extend filopodia up gradients of the chemoattractant, unless c) contact inhibition prevents chemotactic filopodium extension. The endothelial cells are polar: cell-cell binding suppresses the extension of chemotactic filopodia, while the cell surfaces in contact with the *ECM* continue to extend filopodia towards the chemoattractant [18]. In our current model, we further assume that *VEGF-A* is not limiting and distributes uniformly over the *ECM*, as in the widely-used human-umbilical-cord vascular-endothelial cell-cultures (*HUVEC*) [5] or in murine or avian yolk sacs [15].

We model endothelial cell behavior at a mesoscopic level using the Cellular Potts Model [19] (*CPM*), a Monte-Carlo approach in which we bias membrane fluctuations and extensions of filopodia according to the concentration of chemoattractant. We describe chemoattractant diffusion macroscopically, using a continuum approximation. An energy-minimization philosophy, a set of constraints and auxiliary conditions determine how the cells move. Intercellular junctions and junctions to the *ECM* determine an adhesive (or binding) energy. Cells move to promote stronger over weaker bonds and shorter rather than longer cell boundaries. An energy constraint regulates cell volume or surface area. Additional constraints or auxiliary conditions easily extend the *CPM* [20, 21, 22, 23]. Because vascular patterns in *HUVEC* cultures and in yolk sacs are essentially monolayers, we use a two-dimensional *CPM*.

The *CPM* represents biological cells as patches of iden-

tical lattice spins $\sigma(\vec{x})$ on a square lattice, where each spin identifies, or “labels” a single biological cell. Connections between neighboring lattice sites of unlike spin $\sigma(\vec{x}) \neq \sigma(\vec{x}')$ represent membrane bonds, where the *bond energy* is $J_{\sigma_{\vec{x}}, \sigma_{\vec{x}'}}$, assuming that the types and number of VE-cadherin and other adhesive cell-surface proteins determine J . An energy penalty increasing with the cell’s deviation from a designated target volume A_σ imposes a *volume constraint* on the biological cells. We define the pattern Hamiltonian:

$$H = \sum_{\vec{x}, \vec{x}'} J_{\sigma_{\vec{x}}, \sigma_{\vec{x}'}} (1 - \delta_{\sigma_{\vec{x}}, \sigma_{\vec{x}'}}) + \lambda \sum_{\sigma} (a_{\sigma} - A_{\sigma})^2, \quad (1)$$

where λ represents a cell’s resistance to compression, and the Kronecker delta is $\delta_{x,y} = \{1, x = y; 0, x \neq y\}$. Each lattice site represents an area of $2 \mu\text{m} \times 2 \mu\text{m}$. We assume that cells do not divide or grow during patterning, with $A_\sigma = 50$ lattice sites and $\lambda = 25$ for all cells. The cells reside in an ECM which is a generalized CPM cell without a volume constraint and with $\sigma = 0$. We use a bond energy $J_{cc} = 40$ between the endothelial cells, and $J_{cM} = 20$ between the endothelial cells and the ECM; for these settings the cells do not adhere without chemotaxis. We define a special, high *cell-border energy* $J_{cB} = 100$ to prevent cells from adhering to the boundaries.

To mimic cytoskeletally driven membrane fluctuations, we randomly choose a lattice site, \vec{x} , and attempt to copy its spin $\sigma_{\vec{x}}$ into a randomly chosen neighboring lattice site \vec{x}' . For better isotropy we use the twenty, first to fourth nearest neighbors [24]. During a *Monte Carlo Step (MCS)* we carry out n copy attempts, with n the number of sites in the lattice. We set the time per MCS at 30 s. We calculate how much the Hamiltonian would change if we performed the copy, and accept the attempt with probability:

$$P(\Delta H) = \{e^{\frac{-\Delta H}{T}}, \Delta H \geq 0; 1, \Delta H < 0\}. \quad (2)$$

All our simulations use a Boltzmann temperature $T = 50$.

In analogy to a previous PDE approach for *in vitro* vasculogenesis [5, 6], the diffusion and secretion of the chemoattractant evolves according to:

$$\frac{\partial c}{\partial t} = \alpha \delta_{\sigma_{\vec{x}}, 0} - (1 - \delta_{\sigma_{\vec{x}}, 0})\epsilon c + D\nabla^2 c, \quad (3)$$

where $\delta_{\sigma_{\vec{x}}, 0} = 1$ inside the cells. $\alpha = 10^{-3}$ is the rate at which the cells release chemoattractant, $\epsilon = \alpha$ is the decay rate of the chemoattractant, and $D = 10^{-13}$. Every site within the CPM cells secretes the chemoattractant, which only decays in the ECM. We solve this PDE numerically using a finite-difference scheme on a lattice that matches the CPM lattice, using 15 diffusion steps per MCS with $\Delta t = 2$ s. For these parameters, the chemoattractant diffuses more rapidly than the cells, enabling us to ignore advection as the cells push the ECM.

We implement preferential extension of filopodia in the direction of chemoattractant gradients [18] by allowing for an extra energy drop at the time of copying [20]:

$$\Delta H_{\text{chemotaxis}} = -\mu(c(\vec{x}') - c(\vec{x})), \quad (4)$$

where \vec{x}' is the neighbor into which site \vec{x} copies its spin, and $\mu = \chi_{cM}$ and $\mu = \chi_{cc}$ at cell-ECM and cell-cell interfaces respectively. We use a value of $\chi_{cM} = 500$, while setting $\chi_{cc} = 0$ ensures that chemotactic extensions occur only at cell-matrix interfaces, reflecting VE-cadherin’s suppression of filopodia. With this method the cells have a biologically realistic, overdamped force-velocity response unlike in previous models which assumed that cells accelerate in chemoattractant gradients [5, 6].

Fig. 1 shows typical simulated vasculogenesis. We randomly distributed 1000 endothelial cells over an area of 333×333 lattice sites, which we positioned in larger lattice of 500×500 to minimize boundary effects. The endothelial cells assembled into a structure resembling a capillary plexus: *chords* of cells enclose *lacunae* which reach a uniform size over time. Smaller lacunae shrink and disappear, while the subdivision of larger lacunae resembles angiogenic sprouting [30] as *e.g.* in the quail yolk sac [25].

In Fig. 2 we initiate the simulation with a mass of endothelial cells, keeping all other parameters the same.

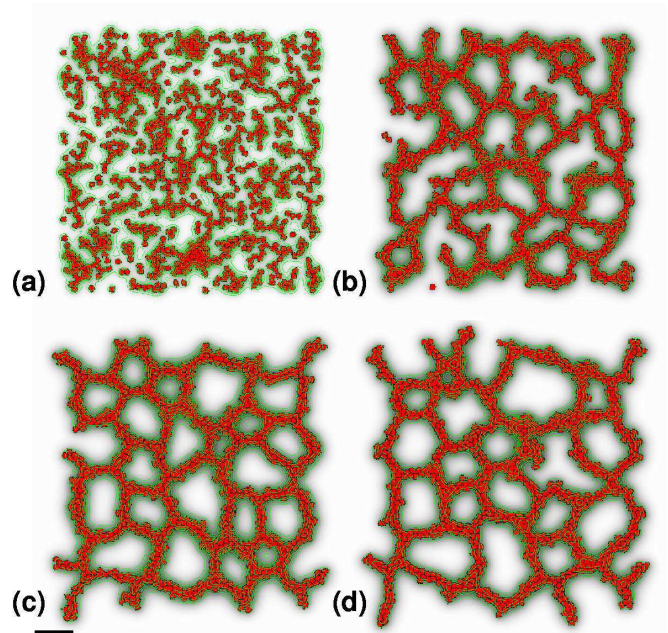


FIG. 1: Vascular network formation in a simulation initiated with 1000 scattered endothelial cells: (a) 10 Monte Carlo Steps (MCS); (b) 1000 MCS; (c) 5000 MCS; (d) 10000 MCS. Scale bar: 50 sites ($\approx 100 \mu\text{m}$). Contour lines (green) indicate ten chemoattractant levels relative to the maximum concentration in the simulation. The greyscale indicates absolute concentration on a logarithmic scale.

After an initial “roughening,” the blob’s surface digitates into a structure reminiscent of a primary capillary plexus (Fig. 2 (d)), the first structure to develop both in sprouting angiogenesis and in vasculogenesis [25]. Thus in our simulation vasculogenesis and angiogenesis are two manifestations of a single process at the level of ECs.

In Fig. 3 we disrupt contact-inhibition by setting $\chi_{cc} = \chi_{cM}$, thus mimicking a VE-cadherin $-/-$ loss-of-function mutation, and allowing for chemotactic filopodia both at cell-ECM and at cell-cell interfaces. In this case, a vascular network no longer forms (Fig. 3(a)). The cells aggregate into small “islands,” as they do in yolk sacs of VE-cadherin $-/-$ mice [15]. The sprouting instability also disappears (Fig. 4(b)); experimentally, VE-cadherin $-/-$ mice have limited angiogenic extensions, in particular in the yolk sac [15].

These results suggest a mechanism by which contact-inhibited directed migration can drive blood vessel sprouting. Around the cluster, the chemoattractant has an exponential profile: the gradient is shallow outside the cluster and becomes steeper in the interior, while it levels off in the center. Thus, surface cells closer to the center push inward more strongly than more peripheral surface cells, which thus move outwards. The balance between the inward, chemotactic force and the outward force determines the direction in which surface cells move. Without contact-inhibition the interior cells also attempt to migrate inwards, thus resisting displacement by the surface cells.

To further test this idea, we varied the chemotactic response at cell-cell interfaces, χ_{cc} . For larger χ_{cc} the internal cells’ chemotaxis cause them to behave as a solid body. We looked for sprouting in cells masses of 128 cells

placed in a 200×200 lattice, keeping all other parameter unchanged. We measured the clusters’ compactness after 10000 MCS, as $C = A_{\text{cluster}}/A_{\text{hull}}$, the ratio between a cluster’s area and its convex hull, as a function of the chemotactic response at cell-cell interfaces relative to chemotaxis at cell-ECM interfaces (χ_{cc}/χ_{cM}). We found a phase transition at $\chi_{cc}/\chi_{cM} \approx 0.5$ separating sprouting from non-sprouting clusters (Fig. 4).

Our current model ignores the possible roles of cell-adhesion, saturation of chemotactic receptors [23], cell elongation [26] and absolute chemotactic response (χ_{cM}); we will present full studies of these parameters elsewhere.

Previous work has treated vasculogenesis and angiogenesis as separate phenomena. Continuum approaches explain vasculogenesis by assuming that ECs actively move along VEGF-A gradients [5, 6, 10]. Purely mechanical models assume that ECs exert stresses on the ECM [7, 8], thus pulling the surrounding ECs towards them. A more recent model also includes active haptotactic migration [9]. Because these mechanical models assume that the stresses exerted on the ECM are radially symmetric, the generic mechanism behind both approaches is similar and involves movement of ECs up either chemical or mechanical gradients around cells and cell clusters. Consequently, the patterning mechanism we described here would likely hold if we assumed mechanical, instead of chemical gradients.

Many models of sprouting angiogenesis represent vessels as interconnected lattice patterns, line segments, or continuous curves, thus explicitly introducing blood-vessel-level phenomenology through a high-level rule for side-branching [11, 12, 13] or branch splitting [27], which experiments do not support. Our model does

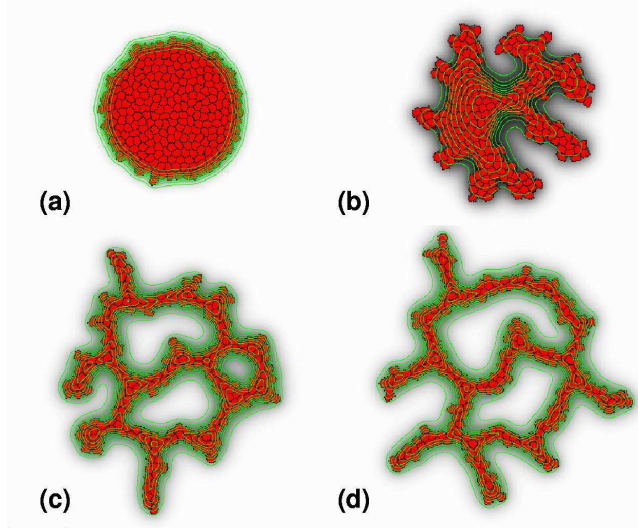


FIG. 2: Sprouting instability in a simulation initiated with a clump of endothelial cells: (a) 10 MCS; (b) 1000 MCS; (c) 5000 MCS; (d) 10000 MCS. Scale bar: 50 sites ($\approx 100 \mu\text{m}$).

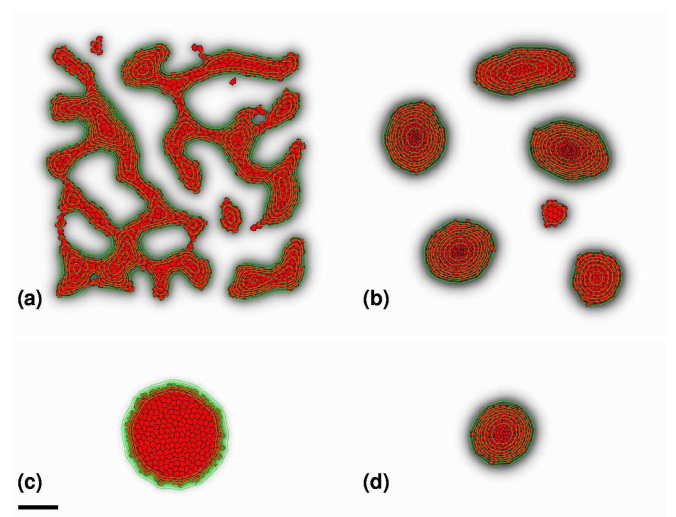


FIG. 3: Disrupted vasculogenesis (a,b) and angiogenesis (c,d) in a simulation without contact-inhibition of motility ($\chi_{cc}/\chi_{cM} = 1$). (a,c) 1000 MCS, (b,d) 10000 MCS. Scale bar: 50 sites ($\approx 100 \mu\text{m}$).

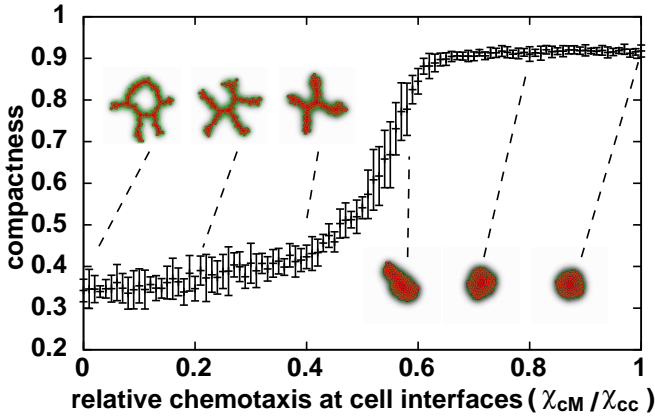


FIG. 4: Compactness ($C = A_{\text{cluster}}/A_{\text{hull}}$) of 128-cell clusters after 10000 MCS (≈ 80 h) as a function of the relative chemotactic response at cell-cell interfaces. Errorbars: standard deviation over ten simulations.

not need such vessel-level phenomenology; the observed branching instability and pattern formation require only experimentally-observed phenomenology at the level of individual ECs. Branching vessel structures emerge from EC phenomenology. Continuum partial differential equation (e.g. [28]) or locally-coupled map lattice (e.g. [29]) approaches to angiogenesis concentrate on blood-vessel density rather than vessel morphology.

Our current work focuses on instability of EC clusters, ignoring the directed blood-vessel sprouting along morphogen gradients that other angiogenesis models consider. Future models will include directed sprouting, e.g. by including additional chemoattractants or chemorepellants in our models.

We gratefully acknowledge discussions with Stuart Newman and András Czirók. R.M. developed parts of the simulation software during work with Paulien Hogeweg at Utrecht University, The Netherlands. This work received support from NSF grants IBN-0083653, NASA Glenn Research Center NAG 2-1619, a Pervasive Technologies Laboratories Fellowship (Indiana University Bloomington), an IBM Innovation Institute Award, the IU Biocomplexity Institute and the IU AVIDD program.

F71 (2001).

- [4] B. S. Kim, J. Chen, T. Weinstein, E. Noiri, and M. S. Goligorsky, *J. Am. Soc. Nephrol.* **13**, 2027 (2002).
- [5] A. Gamba, D. Ambrosi, A. Coniglio, A. De Candia, S. Di Talia, E. Giraudo, G. Serini, L. Preziosi, and F. Bussolino, *Phys. Rev. Lett.* **90**, 118101 (2003).
- [6] G. Serini, D. Ambrosi, E. Giraudo, A. Gamba, L. Preziosi, and F. Bussolino, *EMBO J.* **22**, 1771 (2003).
- [7] D. Manoussaki, S. R. Lubkin, R. B. Vernon, and J. D. Murray, *Acta Biotheor.* **44**, 271 (1996).
- [8] J. D. Murray, *C. R. Biol.* **326**, 239 (2003).
- [9] P. Namy, J. Ohayon, and P. Tracqui, *J. Theor. Biol.* **227**, 103 (2004).
- [10] D. Ambrosi, A. Gamba, and G. Serini, *B. Math. Biol.* **66**, 1851 (2004).
- [11] A. R. A. Anderson and M. A. J. Chaplain, *B. Math. Biol.* **60**, 857 (1998).
- [12] S. R. McDougall, A. R. A. Anderson, M. A. J. Chaplain, and J. A. Sherratt, *B. Math. Biol.* **64**, 673 (2002).
- [13] S. Tong and F. Yuan, *Microvasc. Res.* **61**, 14 (2001).
- [14] P. Carmeliet, *Nat. Med.* **6**, 389 (2000).
- [15] S. Gory-Fauré, M.-H. Prandini, H. Pointu, V. Roullet, I. Pignot-Paintrand, M. Vernet, and P. Huber, *Development* **126**, 2093 (1999).
- [16] E. Dejana, *Nat. Rev. Mol. Cell Bio.* **5**, 261 (2004).
- [17] L. Lamalice, F. Houle, G. Jourdan, and J. Huot, *Oncogene* **23**, 434 (2004).
- [18] H. Gerhardt, M. Golding, M. Fruttiger, C. Ruhrberg, A. Lundkvist, A. Abramsson, M. Jeltsch, C. Mitchell, K. Alitalo, D. Shima, et al., *J. Cell Biol.* **161**, 1163 (2003).
- [19] J. A. Glazier and F. Graner, *Phys. Rev. E* **47**, 2128 (1993).
- [20] N. J. Savill and P. Hogeweg, *J. Theor. Biol.* **184**, 229 (1997).
- [21] P. Hogeweg, *J. Theor. Biol.* **203**, 317 (2000).
- [22] M. Zajac, G. L. Jones, and J. A. Glazier, *Phys. Rev. Lett.* **85**, 2022 (2000).
- [23] R. M. H. Merks, S. A. Newman, and J. A. Glazier, *Lect. Notes Comput. Sc.* **3305**, 425 (2004).
- [24] E. A. Holm, J. A. Glazier, D. J. Srolovitz, and G. S. Grest, *Phys. Rev. A* **43**, 2662 (1991).
- [25] W. Riese, *Nature* **386**, 671 (1997).
- [26] R. M. H. Merks, S. V. Brodsky, M. S. Goligorsky, S. A. Newman, and J. A. Glazier, submitted.
- [27] S. Y. Sun, M. F. Wheeler, M. Obeyesekere, and C. W. Patrick, *B. Math. Biol.* **67**, 313 (2005).
- [28] H. M. Byrne and M. A. J. Chaplain, *B. Math. Biol.* **57**, 461 (1995).
- [29] B. Capogrosso Sansone, M. Scalerandi, and C. A. Condat, *Phys. Rev. Lett.* **87**, 128102 (2001).
- [30] See EPAPS Document No. [number] will be inserted by publisher] (temporarily at <http://www.science.uva.nl/~roel/IU/PRL/>) for movies of the simulations in Figs. 1-3. A direct link to this document may be found in the online article's HTML reference section. The document may also be reached via the EPAPS homepage (<http://www.aip.org/pubservs/epaps.html>) or from <ftp://aip.org> in the directory /epaps/. See the EPAPS homepage for more information

* Electronic address: post@roelandmerks.nl

† Electronic address: glazier@indiana.edu

- [1] S. Liekens, E. De Clerq, and J. Neyts, *Biochem. Pharmacol.* **61**, 253 (2001).
- [2] P. Carmeliet and R. K. Jain, *Nature* **407**, 249 (2000).
- [3] J. Chen, S. Brodsky, H. Li, D. J. Hampel, T. Miyata, T. Weinstein, U. Gafter, J. T. Norman, L. G. Fine, and M. S. Goligorsky, *Am. J. Physiol.-Renal Physiol.* **281**,